

# Deposition of Ti-Based Thin Films on AISI 1020 Steel Substrates Using the Cathodic Cage Plasma Deposition Technique

Raul Felipe Barros da Silva<sup>a</sup>, Wandercleiton Cardoso<sup>b\*</sup> , Leonardo Cabral Gontijo<sup>a</sup>,  
Bruno Poubel Pimentel<sup>a</sup>, Pedro Rufp Pereira Viana<sup>c</sup>, André Gustavo de Sousa Galdino<sup>b</sup>

<sup>a</sup>Instituto Federal de Educação Ciência e Tecnologia do Espírito Santo, Vitória, ES, Brasil.

<sup>b</sup>Università degli Studi di Genova, Facoltà di Ingegneria, Genova, Italia.

<sup>c</sup>Universidade Federal do Rio de Janeiro, Laboratório de Ensaio não Destrutivos, Corrosão e Soldagem, Rio de Janeiro, RJ, Brasil.

Received: October 25, 2022; Revised: February 24, 2023; Accepted: March 30, 2023

The automotive industry is one of the largest industrial segments in the world market. The exhaust system of motor vehicles is responsible for the emission and treatment of toxic gasses released by the engine. In this sense, the application of titanium on an AISI 1020 steel substrate was carried out by plasma deposition using a cathode cage. The aim of this research was to evaluate the application of this material in the exhaust system of motor vehicles. The samples were characterized by scanning electron microscopy (SEM), confocal microscopy (CM), microhardness tests and corrosion resistance tests. The samples exhibited a thin film with higher titanium content and hardness than the uncoated sample. The corrosion potential also increased and the current density was lower than the uncoated sample. The conclusion is that the deposition of thin titanium films on AISI 1020 steel with CCPD has the potential to produce thin films.

**Keywords:** *Cathodic cage, Plasma deposition, AISI 1020 steel, thin films, titanium.*

## 1. Introduction

The automotive industry is one of the largest industrial segments in the world market. It ranges from the industry that manufactures the vehicles to the mechanical workshops responsible for the maintenance of cars, motorcycles, busses, trucks and tractors. Regarding this segment, the importance and necessity of an exhaust system for exhaust gasses is highlighted<sup>1-6</sup>.

The exhaust system is the part responsible for the dissipation and treatment of toxic gasses released by the engine and also reduces the noise of the vehicle. Although it is not necessarily thought of when buying a car, it is very important both for the proper functioning of the vehicle and for the protection of the environment. It consists of components connected by exhaust pipes, located between the engine and the exhaust system for the gasses burned by the vehicle<sup>2,4,7-12</sup>.

The main function of the exhaust system is to eliminate the gasses produced after the combustion of the cylinders, that is, to direct the properly filtered gasses out of the vehicle and prevent toxic gasses from entering the interior of the vehicle. Other functions include reducing noise pollution and maintaining good vehicle performance<sup>1,3,4,12-18</sup>. Figure 1 shows an example of a car exhaust system.

Various materials such as stainless steel, low-carbon steel, and cast iron are used in automotive exhaust systems because of their thermal properties. However, they can corrode because the environment of the car exhaust system

is very corrosive, as the exhaust gasses and condensation water contain harmful elements such as Cl<sup>-</sup>, SO<sub>4</sub><sup>2-</sup>, SO<sub>3</sub><sup>2-</sup>, HCO<sup>3-</sup>, CO<sub>3</sub><sup>2-</sup> and CH<sub>3</sub>COOH<sup>1,7,8,19-24</sup>.

These harmful elements affect air quality and can lead to asphyxiation accidents or long-term occupational diseases. Because they are nearly odorless, it is virtually impossible to notice the release of exhaust from vehicles within a few seconds. Therefore, in most cases, workers do not feel the presence of gasses in the air until pollution is more advanced. Exhaust gasses from motor vehicles reach highly toxic levels in a short time, causing symptoms such as nausea, dizziness, burning eyes, malaise, and unconsciousness. Gasses released by vehicles during operation are not only harmful to the respiratory system, but also carcinogenic, especially when come from of diesel engines<sup>3,7,9,25-30</sup>.

For example, the emission of gasses into the atmosphere releases thousands of particles (soot) containing toxic substances such as benzene, arsenic and formaldehyde, which pollute the air. In addition, the heavy emission of CO<sub>2</sub> causes respiratory problems and, in extreme cases, suffocation. Since people can be exposed to these toxic gasses frequently, the consequences are numerous<sup>26,31-36</sup>.

As mentioned earlier, different types of steels and cast irons can be used in car exhaust systems. Although low-carbon steels have low corrosion and wear resistance, they have high toughness, ductility, weldability, and machinability, making them widely advantageous due to their low production cost and market availability, although some properties limit their use in some automotive component manufacturing processes<sup>7,10,15,37-42</sup>.

\*e-mail: wandercleiton.cardoso@dicca.unige.it

Low-carbon steels are used in industry to manufacture automotive sheet, structural sections, pipes, concrete reinforcements and bridges. These classes of materials have a carbon content of up to 0.30%, which means that their surface properties (tribological properties, oxidation and corrosion resistance) are worse than those of other steel grades. To improve the surface properties of steels, some processes are used, such as heat treatment processes, carburizing, nitriding, nitrocarburizing, boriding and plasma spraying<sup>43-48</sup>.

Nitriding is a thermochemical treatment that increases the surface hardness, fatigue resistance, wear resistance and, in certain cases, corrosion resistance of steels. Generally, the nitrided surface can be seen under an optical microscope as a layer of compounds commonly referred to as a white layer in the outermost part of the surface, followed by the diffusion zone. The nitriding processes traditionally used in industry, which are distinguished by the nitriding medium, are gas nitriding and salt bath nitriding, but plasma nitriding has gained importance in the last decade in the processing of special steels<sup>49-54</sup>.

The main advantage of plasma nitriding is the possibility to control the metallurgy of the nitrided layer. For the same steel, this process can be used to vary the type of nitride formed in the compound layer and even prevent its formation. For this purpose, the composition of the gas mixture, the temperature and the nitriding time must be precisely controlled. The nitriding depth is controlled by controlling the temperature and the process time. Nitriding without a compound layer is performed with a low nitrogen potential and/or short nitriding times. Increasing the nitrogen potential and adding methane preferably leads to the formation of a layer of (3N-Fe<sub>2</sub>) type nitride compounds. It is very important to remember that the chemical composition of the substrate plays an important role in the metallurgy of the nitrided surface<sup>47,49,55-60</sup>.

Plasma nitriding is performed under low-pressure glow discharge at temperatures ranging from 375 to 560°C to improve the surface hardness and wear resistance of steels. Conventional plasma nitriding has a limitation when components with different shapes or surface-to-mass ratios are subjected to varying degrees of ion bombardment, resulting in inhomogeneous hardness and depth of nitrogen diffusion after plasma nitriding. These limitations have been reduced with the development of new techniques, post-discharge nitriding, plasma ion implantation, and active screen nitriding<sup>6,15,24,39,61-64</sup>.

Ionic plasma nitriding has limitations such as edge effects and overheating that occur with thermochemical plasma treatment and are due to the high surface-to-volume ratio, especially for parts with complex geometry. This limitation was eliminated using cathode cages, since the plasma was formed in the cage rather than directly in the samples, and the treatment temperature was reached by radiating the heat supplied by the heated cage<sup>65-68</sup>.

Ceramic materials are used to coat metals because of their properties such as high melting point and high corrosion and wear resistance compared to metals. Ceramic applications include stacks of anti-reflective coatings and UV protective films in glazing for the automotive industry, knock sensors,

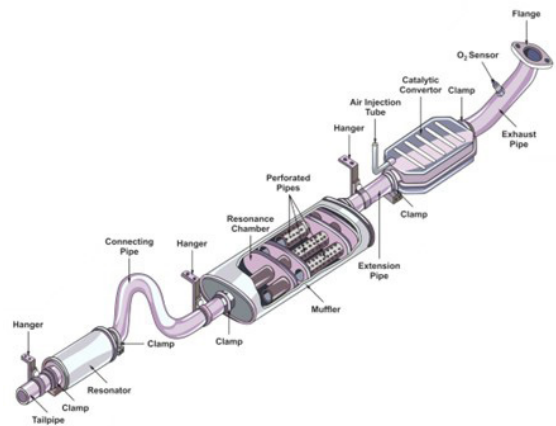


**Figure 1.** Example of an automotive exhaust system.

oxygen sensors and exhaust catalysts for the automotive industry, bioceramic films for metal alloys, coatings, thin films and plasma spray, however it is also used stainless steels and magnesium alloys whenever corrosion protection is a determining factor. In this new scenario of Industry 4.0 growth, several authors write about new techniques to produce steels with higher quality<sup>1,5,9,18,26,30,32,40,58,69-73</sup>.

In recent years, the study of plasma nitriding of metals and non-ferrous alloys such as titanium and aluminum has intensified. Titanium is a light metal with excellent mechanical properties. Therefore, the automotive and aerospace industries have made large investments in the development of titanium nitriding. Nitriding has enabled an improvement in wear resistance and expanded the use of this material in these industry segments. In this context, this paper aims to coat and characterize AISI 1020 steel with thin films based on Titanium pure and titanium dioxide deposited by cathode cage plasma nitriding (CCPD).

## 2. Experimental Method

### 2.1. Sample preparation

The following materials were used for this study: 1) commercial AISI 1020 steel, which was used as a substrate; 2) wires and strips, grade 2, of pure titanium; and 3) anatase titanium dioxide. The titanium strips were used to fabricate the cathode cage, while titanium wire and anatase titanium dioxide were used to coat the samples. The choice of titanium was based on the literature, as there are several similar works in which titanium is used to coat stainless steel and carbon due to its wear and corrosion resistance.

First, sixteen cylindrical samples with dimensions Ø25.4 x 10.0 mm were fabricated from AISI 1020 steel. Then these samples were ground on paper with grits of 80, 120, 220, 320, 400, 600 and 1200, and then polished with alumina suspension paste (1 and 0.3 µm) until they obtained a mirror-smooth surface. The samples were cleaned in water and ethanol with dry ultrasound at 23°C and then examined under an optical microscope to ensure that they were risk-free.

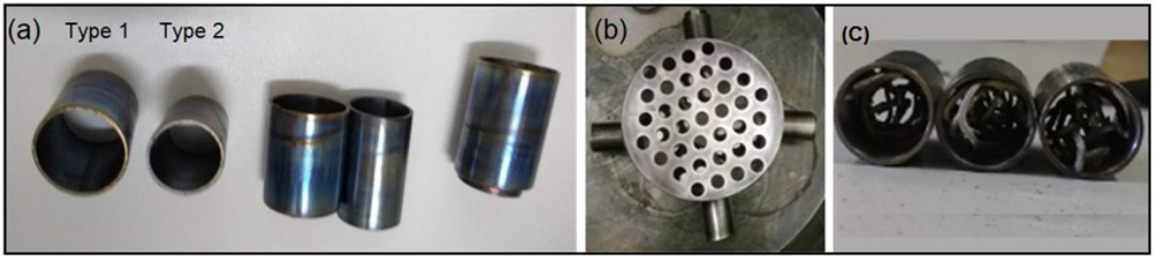


**Figure 2.** (a) Types of tubes; (b) cathode cage; (c) tube assembly scheme.

After polishing, the sixteen samples were divided into four groups of four samples each. In the first group, the four samples were completely covered with Kapton® brand thermoresistant polymer tape (sample A). In the second group, another four samples were partially covered and these samples were not covered with thin film (sample B). In the third group, another four samples were partially coated and for these samples, the addition of a titanium thin film was planned (sample C). In the fourth and final group, another four samples were partially coated and for these samples, the addition of a thin film titanium oxide was planned (sample D).

## 2.2. Cathodic Cage Plasma Deposition (CCPD)

A cylindrical cathode cage with a lid with holes and side tubes was used. When assembling the cathode cage, type two tubes were inserted into type 1 tubes and then into the side holes of the cathode cage. Table 1 shows the basic dimensions of the cathode cage, while Figure 2 shows the cathode cage and the tubes used in detail.

The main function of this cathode cage is its versatility, because depending on the treatment conditions, such as gas, temperature, dopants and pressure, the material deposition is improved and the film is more uniform. In this study, two tubes were used (Figure 2) because this type of configuration increases the deposition rate, as shown by initial experiments.

Plasma deposition in cathodic cage was performed in four different steps. In the first stage, the deposition was performed on four samples completely covered with Kapton® tape and no additional material was considered. In the second stage, the deposition was performed on four samples that were partially covered with Kapton® tape, and no additional material was considered either. In the third stage, deposition was performed on four samples partially covered with Kapton® tape, using solid titanium wires inserted in tubes (type 2). In the fourth stage, another four samples were partially covered with Kapton® tape and then 0.500 g of powdered titanium dioxide was added to type 2 tubes, which were inserted into type 1 tubes and mounted on the cathode cage.

The solid titanium wire and the titanium dioxide powder are not in a buoyancy potential inside the cathode cage, because a completely different plasma process takes place, since the tubes enhance the discharge process of the hollow cathode inside the tubes and the pullout sputtering is high for titanium wires and even higher for titanium dioxide powder. The energy required for this propagation depends on the binding energy of the individual substances.

**Table 1.** Cathode cage dimensions.

Inner diameter	Ø 100 mm
Height	50 mm
Number of holes in the lid	37 holes
Number of side holes	04 holes
Dimensions of type 1 side tubes	Ø 15 mm x 30 mm long
Dimensions of type 2 side tubes	Ø 10 mm x 30 mm long

**Table 2.** Parameters used for deposition.

$T_{on}$ [ms]	80–120
Working pressure [Pa]	106.66–123.99
Gas	Hydrogen
Flow rate [l/min]	8.000
$I_m$ [A]	0.53–0.69
Deposition time	6 h after parameters stabilization
Coating	Pure Ti grade 2 and $TiO_2$
$V_m$ [V]	146–153
Temperature [K]	723

Plasma deposition was performed using a SDS reactor model SDSFLUX. The deposition process was performed using the parameters listed in Table 2.  $T_{on}$  represents the period, the parameter that controls the reactor power, which affects the temperature, the average current and the opening of the arcs. The desired pressure is the pressure used in the reactor to deposit the material (internal vacuum), where  $I_m$  and  $V_m$  are the average current and voltage in the reactor, respectively.

The main advantage of using the cathodic cage is mainly the low cost of deposition (both compared to the reactors already present in most laboratories and industries) and maintenance costs. Another important point is the possibility to dope films with different materials. Moreover, the coating can be performed on parts with different dimensions. From the smallest to the largest pieces. After assembling the cathode cage with type 1 and 2 tubes, four samples made of AISI 1020 (Figure 3) were placed in the reactor. They were placed inside the cage away from the walls so that they would not be under the tubes, since the distance between the cathode cage and the sample affects the coating.

Initially, the reactor was connected to hydrogen only and  $T_{on}$  was equal to 30 ms to remove any oxides present in the samples or cathode cage (purification process). After 30 minutes, counting of the deposition time was started.

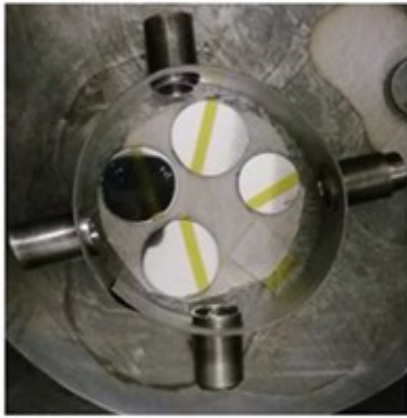


**Figure 3.** Sample positioning.

The Ton was gradually increased every 20 ms up to 120 ms as the rate of temperature rise decreased, i.e., 10 minutes for the 80 ms Ton, 60 minutes for the 100 ms Ton and then for the 120 ms Ton. This procedure was used for all deposition conditions.

### 2.3. Surface characterization of samples

The determination of the chemical composition of the AISI 1020 steel was carried out in an Oxford Instruments Foundry-Master Pro model, while the hardness tests were performed in a Shimadzu DUH 211S dynamic ultramicrohardurometer. In addition, the corrosion test was performed on an Autolab-Metrohm 302N using Nova® 2.1 software.

The chemical composition of the anatase titanium dioxide was determined using a Shimadzu EDX-720 X-ray fluorescence (XRF) instrument. Surface characterization of the samples was performed by scanning electron microscopy (SEM) using a Zeiss EVO MA10 with an Oxford Instruments X-MaxN energy dispersive spectrometer for semi-quantitative determination of the chemical composition of the samples. Quantification of the average chemical composition in three different regions was also performed on all bet groups to check if there were differences in chemical elements in these regions. Only the chemical elements iron, oxygen, and titanium were evaluated.

A topographic evaluation of the Kapton® tape coated sample was performed using a Leica Accurion confocal microscope. The height difference between the film step and the Kapton® tape area was measured. The thickness of the thin film was measured by scanning the sample area with the microscope to create a three-dimensional model of the surface. Relief measurement is possible due to the reflection of light by the irregular topography of the sample in the step between the thin film and the substrate. A topography plot was created showing the height profile (y-axis) as a function of the linear position of the sample (x-axis).

The microhardness tests were performed using a Shimadzu DUH 211S dynamic ultramicrodurimeter. The force used for the test was 50 mN. The substrate hardness and thin film hardness were measured. To ensure good randomness of the measurements, seven wells were created in each sample. To avoid points that could have very different hardness values and to ensure the reliability of the test, the measurements were taken in the central area of the sample.

**Table 3.** Parameters used for corrosion tests.

Initial potential [V]	- 0.70
Final potential [V]	+ 0.70
Scanning speed [V/s]	0.001
Step [V]	0.005
Reference electrode	Calomel
Counter electrode	Platinum

**Table 4.** Chemical composition of AISI 1020 steel (wt%).

Chemical element	Chemical composition (wt%)	Chemical composition UNS G10200 (wt%)
C	0.21	0.17–0.23
Mn	0.52	0.30–0.60
P	0.02	≤ 0.040
S	0.02	≤ 0.050
Si	0.11	-
Cr	0.10	-
Mo	0.02	-
Ni	0.06	-
Cu	0.29	-
Ti	< 0.01	-
Fe	Balance	Balance

**Table 5.** Chemical composition of TiO<sub>2</sub>.

Chemical	Chemical composition (wt%)
TiO <sub>2</sub>	99.03
Al <sub>2</sub> O <sub>3</sub>	0.41
SiO <sub>2</sub>	0.28
P <sub>2</sub> O <sub>5</sub>	0.28

After a measurement, the instrument microscope was moved to another area so that the previous measurement could not be seen, and the next measurement was taken until all impressions were completed.

Corrosion tests were performed in an Autolab-Metrohm 302N instrument and analyzed in Nova® 2.1 software. For the potentiodynamic polarization studies, the samples with and without titanium-based thin films were immersed in a 3.5% NaCl solution. The analysis of the potentiodynamic polarization curve was performed with a classical three-electrode setup and the parameters are listed in Table 3.

## 3. Results and Discussion

### 3.1. Materials chemical composition

The chemical composition of the AISI 1020 steel was compared with that of the UNS G10200 datasheet (Table 4). It was found that the substrate without deposits had a low titanium content.

The chemical composition of anatase titanium dioxide (TiO<sub>2</sub>) is illustrated in Table 5, which indicates 99% by weight of TiO<sub>2</sub> and 1% by weight of impurities.

### 3.2. Surface characterization of samples

The result of the deposition is shown in Figure 3. The samples have changed in their natural color. The samples have changed from gray (Figure 3a) to a bluish color with golden areas at the edges (Figure 3c and 3d), and as seen in the area where the Kapton® tape was located, according in Figure 3b. These changes in the esthetics of the samples to which the film was applied prove that this effect, as shown in Figure 3b and 3c, is due to the use of Kapton® tape.

SEM and energy-dispersive X-ray spectroscopy (EDS) were performed on the samples to determine the chemical composition of some regions of the sample deposited to confirm the existence of the thin film. The EDS average chemical composition is presented in Table 6.

In conditions B, C, and D, the amounts of oxygen and titanium determined using EDS were higher than in condition A. However, it is not possible to determine that all of the measured oxygen came from the formation of titanium oxide because EDS does not accurately identify oxygen. However, it is possible that the samples were oxidized during the deposition process, resulting in low levels of iron oxide and titanium oxide. The amounts of iron detected in the samples were low and EDS detected at least 0.1% titanium in the samples.

Although the chemical compositions were similar, the microscopic images were different. For sample A, there was almost no difference in the coloration of the samples, but for the deposited samples B, C, and D, a gradual increase in lighter spots and holes was observed on the surface of the samples, probably related to the relief of the sample from the deposited film of sample A.

A higher percentage of titanium was observed in the area of the samples that contained only the film than in Sample A (without Ti content), as well as compared to the percentages of this element in the area that contained Kapton® tape. Since there was no indication of the presence of Ti in the areas with Kapton® tape, the presence of this element in the deposition areas of the film suggests that this element

is only from the cathodic cage and deposition processes. It is noteworthy that the percentage amount of oxygen in the areas containing the titanium film is much greater than the amount of this element measured in the Kapton® tape covered area of the sample, indicating the formation of at least partial TiO<sub>2</sub> on the deposited titanium.

### 3.3. Topographical evaluation

The thickness of the deposited layers was measured as height difference (Dz) using a confocal microscope. Table 7 summarizes the results of the layer thicknesses for samples B, C and D. It is worth noting that the generated layer for sample B is quite heterogeneous, as the standard deviation corresponds to about 5% (standard deviation divided by the mean) of found layer thickness. The layer thickness values found for sample C are close to those of sample B, but with a much lower standard deviation than those of samples B and D. It can be seen that sample D has an average layer thickness that is 2.5 times greater than that of samples B and C.

The measurements presented in Table 7 show that the thin film was indeed deposited, as evidenced by the height difference between the planes, indicating that titanium deposition did indeed occur in the area without Kapton® tape, and confirmed by the results from EDS. Figure 4 shows a topographic view of sample B with Kapton® tape. Figure 5a shows the difference between the regions with and without deposition, while Figure 5b shows the step created by the Kapton® tape, where differences in relief and topography can be observed.

Figure 5 shows some differences between the regions with the film applied (left region) and the region covered with Kapton® tape (right). The region covered with the film has a more pronounced relief, possibly due to the cathodic spraying to which the sample was exposed during deposition. In addition to the step, the relief of the sample increases when the Kapton® tape is removed, as shown in Figure 4b. In all techniques, whether magnetron sputtering or filtered cathodic arc deposition, which are deposition techniques praised by the quality of the films, heterogeneities occur in the films. In this technique, the heterogeneity of the films is much more pronounced, mainly because the materials used in the production of the cathodic cages and the dopants are not of high purity. Moreover, since the pressures are very high compared to other techniques, homogeneous layers cannot be obtained. It is important to point out that this technique is not intended to replace other processes such as magnetron sputtering and filtered cathodic arc deposition, but is an option for many laboratories and industries that need to coat parts with different dimensions.

**Table 6.** Results of EDS measurements of Samples.

Chemical Element	Sample A	Sample B	Sample C	Sample D
Fe	99.6 ± 0.2	95.0 ± 0.2	95.0 ± 0.2	96.4 ± 0.2
O	0.4 ± 0.2	4.7 ± 0.2	4.7 ± 0.2	3.5 ± 0.2
Ti	-	0.3 ± 0.1	0.3 ± 0.1	0.1 ± 0.1

Sample A = 100% Kapton® tape and no thin film; Sample B = Partial Kapton® tape and no thin film; Sample C = Partial Kapton® tape and titanium thin film; Sample D = Partial Kapton® tape and titanium dioxide thin film.

**Table 7.** Film thickness results.

Sample	Sample B	Sample C	Sample D
	Dz (nm)	Dz (nm)	Dz (nm)
1	138.27	119.33	316.62
2	101.65	116.18	304.23
3	149.12	129.53	291.68
4	126.30	117.61	300.66
Average ± standard deviation	128.84 ± 20.38	120.66 ± 6.05	303.30 ± 10.33

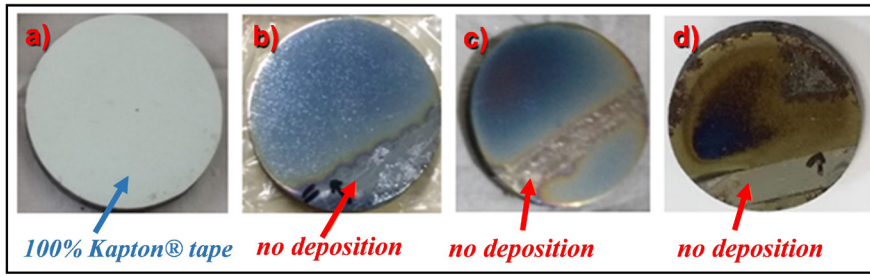


Figure 4. Samples after deposition.

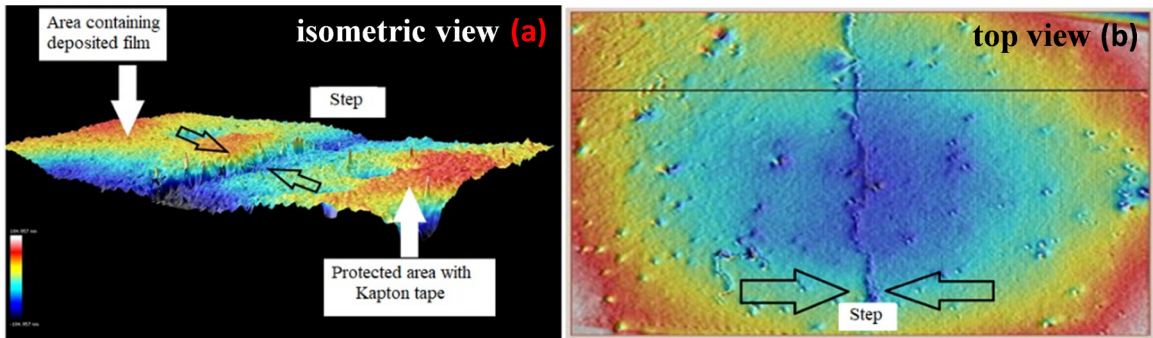


Figure 5. Topographic view of Sample B.

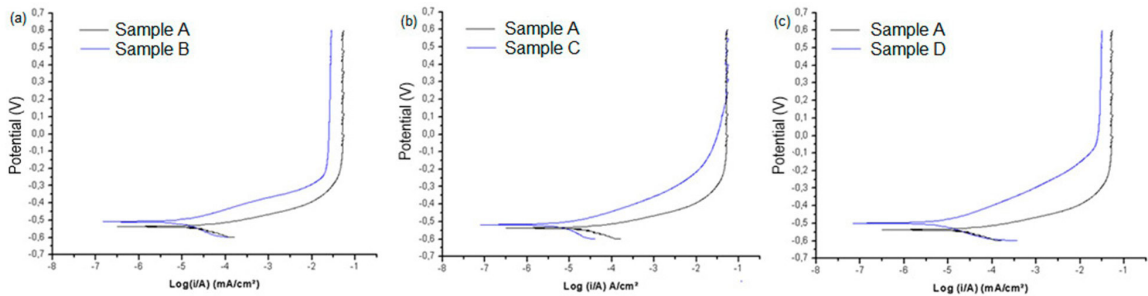


Figure 6. Polarization curves.

### 3.4. Hardness tests

When looking at the hardness values of the substrate, it can be seen that the standard deviation of the hardness values at all measuring points was low. This was to be expected since the AISI 1020 steel has a low tendency to form hard carbides. A total of one hundred and twelve measurements were performed. For each sample, seven measurements were performed. Table 8 shows the result of the measurements considering the mean and standard deviation of seven measurements.

It was observed that the value of standard deviation in samples B and D and some of the reasons that can explain the high standard deviation are the density of the applied film, the thickness of the film at the measurement point and the porosity. However, samples B, C, and D had higher hardness values compared to sample A, with the hardness being two times higher than sample A. The increase in hardness was also observed in the study by other authors<sup>6,20,25,38,46,65</sup> in which the authors used aluminum powder deposited by the

Table 8. Hardness tests.

Sample	Load (mN)	Hardness (HV)
A	50.79 ± 0.17	148.13 ± 03.94
B	50.82 ± 0.16	326.93 ± 37.30
C	50.95 ± 0.01	319.88 ± 15.05
D	50.80 ± 0.15	315.47 ± 44.64

cathode cage method. Other authors<sup>7,11,24,39,65,69</sup> also reported an increase in the hardness of materials coated with a film.

It is important to point out that the substrate always has an influence on the result of a hardness test. On the other hand, although this influence must be taken into account, the work is not mischaracterized because it takes into account the variation of the hardness of the samples compared to the untreated sample, just as the variation of the hardness of the material was observed. As for the hardness tests, it is known that there were four samples for each group.

**Table 9.** Corrosion potential.

Sample	Corrosion potential (V)
A	$-0.55 \pm 0.01$
B	$-0.51 \pm 0.01$
C	$-0.52 \pm 0.01$
D	$-0.51 \pm 0.01$

### 3.5. Corrosion resistance tests

The corrosion potential of sample A is about -0.55 VSCE (Figure 6a), while that of sample B is about -0.51 VSCE (Figure 6b), showing that the surface treatment causes a slight increase in the corrosion potential. To illustrate, at a potential of -0.40 VSCE, the current density of sample B is about  $5.10^{-4}$  A/cm<sup>2</sup>, while the current density of sample A is about  $1.10^{-2}$  A/cm<sup>2</sup>, i.e., the current density of sample B is about twenty times lower than that of sample A.

The same behavior with small differences can be seen in Figures 6b and 6c. Xu et al.<sup>41</sup> and Russo et al.<sup>69</sup> have shown that the corrosion potential increases when TiO<sub>2</sub> is used for coating. According to these authors, the deposition that occurred can be interpreted in terms of a two-layer oxide film model, where the innermost layer is dense and compact and has high corrosion resistance (anatase). The outermost layer has low resistivity, indicating that the material has more defects, is less compact, and has lower corrosion resistance. The polarization curves of the titanium-based treated samples were compared with those of the untreated sample (Sample A) and shown in Figure 6 and then the estimated results are summarized in Table 9

Several authors<sup>8,16</sup> explain that the possible reason for this behavior is the difference between nucleation and growth processes. Such behavior of the passive layer was also cited by other authors<sup>45</sup> in their study. The typical result of titanium in corrosive media is the formation of a protective oxide, but when the electrolyte contains NaOH, the observed behavior is somewhat different. After the initial formation of the oxide film, there is an abrupt decrease in film formation and later a decrease in thickness. This is due to the instability of the film formed on the surface, which causes the potential to become less noble with time and the film becomes thinner<sup>16</sup>.

In the depositions performed in the present study, slightly higher corrosion potentials and lower current densities were obtained in the polarization curves, indicating that the coatings slightly improved the corrosion resistance of the coated samples compared to the AISI 1020 steel in the 3.5% NaCl medium; however, the depositions performed did not show similar results to those of the authors<sup>8,16,45</sup>.

One explanation for the difference in results is related to the medium used, which may have favored the decrease in the thickness of the passive layer mentioned by other authors<sup>8,16,45</sup>. Another reason that could have contributed to this difference in the result was the deposited film, which may not have been as dense and compact as the film layers mentioned by the above authors, which could be due to the deposition process used and the results of the deposition parameters.

## 4. Conclusions

In the present study, the deposition of titanium thin film coatings on an AISI 1020 steel substrate by plasma deposition using a cathode cage was evaluated, and it can be concluded that:

- The coated samples exhibited differences in several properties compared to the standard uncoated samples, from their optical appearance to their mechanical and electrochemical properties.
- The chemical composition of the metallic substrate showed a residual content of titanium and the EDS test showed a content of 0.1% titanium and 1.4% oxygen after deposition, which can be attributed to the deposition of the film.
- The deposition of titanium thin films promoted an increase in the hardness values of AISI 1020 steel, from 148 HV to values above 315 HV.
- Titanium-based samples slightly increased the corrosion potential, but this increase did not imply a significant change from a thermodynamic point of view. However, the current densities of the titanium-based samples were significantly reduced compared to the samples without coating, and the results presented in Table 8 confirm that coated titanium-based materials have better corrosion resistance.
- It was possible to observe an increase in thickness between the uncoated region and the titanium coating, ranging from 120 to 310 nm.

## 5. References

1. Cardoso W, Baptista R, Di Felice R. Mathematical modeling of a solid oxide fuel cell operating on biogas. *Bull Electr Eng Inf.* 2021;10(6):2929-42.
2. Guarnaccio A, Belviso C, Montano P, Toschi F, Orlando S, Ciaccio G, et al. Femtosecond laser surface texturing of polypropylene copolymer for automotive paint applications. *Surf Coat Tech.* 2021;406:126727.
3. Ipke AE, Orhorhoro EK, Gobir A. Engineering material selection for automotive exhaust systems using CES software. *Int J Eng Technol.* 2017;3(2):50-60.
4. Stojanovic B, Glisovic J. Application of ceramic matrix composite in automotive industry. *Encycl Mater Compos.* 2021;2:275-92.
5. Cardoso W, Baptista R. Laves phase precipitation and sigma phase transformation in a duplex stainless steel microalloyed with niobium. *Materia.* 2022;27(2):e13200.
6. Bashir MI, Shafiq M, Naeem M, Zaka-ul-Islam M, Díaz-Guillén JC, Lopez-Badillo CM, et al. Enhanced surface properties of aluminum by PVD-TiN coating combined with cathodic cage plasma nitriding. *Surf Coat Tech.* 2017;327:59-65.
7. Naeem M, Shafiq M, Zaka-ul-Islam M, Bashir MI, Díaz-Guillén JC, Lopez-Badillo CM, et al. Novel duplex cathodic cage plasma nitriding of non-alloyed steel using aluminum and austenite steel cathodic cages. *J Alloys Compd.* 2017;721:307-11.
8. Yamaguchi S, Lee H, Ogura A, Ohshita Y. Improvement in the passivation quality of titanium oxide thin films by doping with tantalum. *Thin Solid Films.* 2021;720:138509.
9. Cardoso W, Machado TAP, Baptista R, Galdino AGS, Pinto FAM, Luz TS. Industrial technological process for welding AISI 301 stainless steel: focus on microstructural control: Smart Innovation, Systems and Technologies. In: 7th Brazilian Technology Symposium, BTSym; 2021 Nov 8-10; Campinas, Brazil. Proceedings. Cham: Springer Nature; 2021. p. 34-41.

10. Krelling AP, Costa CE, Milan JC, Almeida EAS. Micro-abrasive wear mechanisms of borided AISI 1020 steel. *Tribol Int.* 2011;111:234-42.
11. Kulikovskiy V, Ctvrtlik R, Vorliceck V, Filip J, Bohac P, Jastrabik L. Mechanical properties and structure of TiO<sub>2</sub> films deposited on quartz and silicon substrates. *Thin Solid Films.* 2013;542:91-9.
12. Itman A, Cardoso W, Vilarim R, Silva RV, Casteletti LC. Austenitic-ferritic stainless steel containing niobium. *REM Rev Escola Minas.* 2013;66(04):467-71.
13. Bach LX, van Thuan D, Thu VT, Phan TB, Vu NSH, Nam ND. An investigation on titania multilayer coatings for enhanced corrosion resistance of carbon steel in simulated seawater by sol-gel dip coating. *J Mater Res Technol.* 2019;8(6):6400-6.
14. Cardoso W, Di Felice R. A novel committee machine to predict the quantity of impurities in hot metal produced in blast furnace. *Comput Chem Eng.* 2022;163(2):107814.
15. Almeida PRQ, Serra PLC, Danelon MR, Rossino LS, Costa THC, Feitor MC, et al. Plasma duplex treatment influence on the tribological properties of the UNS S32760 stainless steel. *Surf Coat Tech.* 2021;426:127774.
16. Fazlinezhad S, Jafarzadeh K, Gugtapeh HS, Mirali SM. Characterization and electrochemical properties of stable Ni<sub>2</sub><sup>+</sup> and F<sup>-</sup> co-doped PbO<sub>2</sub> coating on titanium substrate. *J Electroanal Chem.* 2022;909:116145.
17. Babur MZ, Iqbal Z, Shafiq M, Naz MY, Makhlof MM. Hybrid TiN-CCPN coating of AISI-201 stainless steel by physical vapor deposition combined with cathodic cage plasma nitriding for improved tribological properties. *J Build Eng.* 2022;45:103512.
18. Cardoso W, Di Felice R, Baptista R. A critical overview of development and innovations in biogas upgrading. In: 7th Brazilian Technology Symposium, BTSym; 2021 Nov 8-10; Campinas, Brazil. Proceedings. Cham: Springer Nature; 2021. p. 42-50.
19. Huang HH, Shiau DK, Chen CS, Chang J-H, Wang S, Pan H, et al. Nitrogen plasma immersion ion implantation treatment to enhance corrosion resistance, bone cell growth, and antibacterial adhesion of Ti-6Al-4V alloy in dental applications. *Surf Coat Tech.* 2019;365:179-88.
20. Naeem M, Fortaleza VC, Serra P, Lima CL, Costa THC, Sousa RRM, et al. Synthesis of molybdenum oxide on AISI-316 steel using cathodic cage plasma deposition at cathodic and floating potential. *Surf Coat Tech.* 2021;406:126650.
21. Kornienko E, Gulyaev I, Smirnov A, Nikulina A, Ruktuev A, Kuzmin V, et al. Microstructure and properties of Ni-Al coatings obtained by conventional and high-velocity atmospheric plasma spraying. *Results Surf Interfaces.* 2022;06:100038.
22. Zavareh MA, Sarhan AADM, Razak BBA, Basirun WJ. Plasma thermal spray of ceramic oxide coating on carbon steel with enhanced wear and corrosion resistance for oil and gas applications. *Ceram Int.* 2014;40(9):14267-77.
23. Itman A Fo, Silva RV, Cardoso WS, Casteletti LC, et al. Effect of niobium in the phase transformation and corrosion resistance of one austenitic-ferritic stainless steel. *Mater Res.* 2014;17(4):801-6.
24. Naeem M, Shafiq M, Zaka-UI-Islam M, Díaz-Guillén JC, Lopez-Badillo CM, Ullah N, et al. Improved surface properties of AISI-304 by novel duplex cathodic cage plasma nitriding. *Mater Lett.* 2017;189:213-6.
25. Naeem M, Zaka-ul-Islam M, Shafiq M, Bashir MI, Díaz-Guillén JC, Zakaullah M. Influence of cathodic cage diameter on mechanical properties of plasma nitrated AISI 304 steel. *Surf Coat Tech.* 2017;309:738-48.
26. Cardoso W, Di Felice R, Baptista RC. Perspectives on the Sustainable Steel Production Process: A Critical Review of the Carbon Dioxide (CO<sub>2</sub>) to Methane (CH<sub>4</sub>) Conversion Process. In: García Márquez FP, Lev B, editors. *Sustainability.* New York: Springer; 2023. p. 361-91. (International Series in Operations Research & Management Science; 333).
27. Lopes RF, Costa JAP, Silva W, Viana BC, Marciano FR, Lobo AO, et al. TiO<sub>2</sub> anti-corrosive thin films on duplex stainless steel grown using cathodic cage plasma deposition. *Surf Coat Tech.* 2018;347:136-41.
28. Lima ROC, Alves C Jr, Melo ACA, Alves SM, Araújo L Fo. New technique for deposition and thermochemical treatment of small parts with complex geometry applied to machining inserts. *J Mater Res Technol.* 2020;9(6):15811-23.
29. Xu L, Shao C, Tian L, Zhang J, Han Y, Zhao L, et al. Intergranular corrosion behavior of Inconel 625 deposited by CMT/GTAW. *Corros Sci.* 2022;201:110295.
30. Cardoso W, Barros D, Baptista R, Di Felice R. Mathematical modelling to control the chemical composition of blast furnace slag using artificial neural networks and empirical correlation. In: *World Multidisciplinary Civil Engineering-Architecture-Urban Planning Symposium - WMCAUS 2021*; 2021; Prague, Czech Republic. Proceedings. Bristol: IOP Publishing; 2021.
31. Minamizawa K, Arakawa J, Akebono H, Nambu K, Nakamura Y, Hayakawa M, et al. el al. Fatigue limit estimation for carburized steels with surface compressive residual stress considering residual stress relaxation. *Int J Fatigue.* 2022;160:106846.
32. Cardoso W, Baptista R, Di Felice R. Artificial neural network for predicting silicon content in the hot metal produced in a blast furnace fueled by metallurgical coke. *Mater Res.* 2022;25:20210439.
33. Movassagh-Alanagh F, Mahdavi M. Improving wear and corrosion resistance of AISI 304 stainless steel by a multilayered nanocomposite Ti/TiN/TiSiN coating. *Surf Interfaces.* 2020;18:100428.
34. Yada K, Watanabe O. Reactive flow simulation of vacuum carburizing by acetylene gas. *Comput Fluids.* 2013;79:65-76.
35. Bedolla-Hernández M, Rosano-Ortega G, Sánchez-Ruiz FJ, Bedolla-Hernández J, Schabes-Retchkiman PS, Vega-Lebrún CA. Electrodeposition mechanism of chromium nanoparticle coatings: modeling and experimental validation. *Chem Eng Sci.* 2022;252:117291.
36. Halim FS, Chandren S, Nur H. Carbon-containing-titania coated stainless steel prepared by high voltage powder spray coating and its adhesion phenomena. *Prog Org Coat.* 2020;147:105782.
37. Kumar A, Bhushan B. Nanomechanical, nanotribological and macrotribological characterization of hard coatings and surface treatment of H-13 steel. *Tribol Int.* 2015;81:149-58.
38. Naeem M, Shafiq M, Zaka-ul-Islam M, Ashiq A, Díaz-Guillén JC, Shahzad M, et al. Enhanced surface properties of plain carbon steel using plasma nitriding with austenitic steel cathodic cage. *Mater Des.* 2016;108:745-53.
39. Naeem M, Torres AVR, Serra PLC, Monção RM, Antônio CA Jr, Rossino LS, et al. Combined plasma treatment of AISI-1045 steel by hastelloy deposition and plasma nitriding. *J Build Eng.* 2022;47:103882.
40. Cardoso W, Di Felice R. Artificial neural networks for modelling and controlling the variables of a blast furnace. In: *IEEE 6th International Forum on Research and Technology for Society and Industry*; 2021 Sep 6-9; Naples, Italy. Proceedings. New York: IEEE; 2021. p. 148-52.
41. Xu Z, Zhang Q, Luo L, Liu Y, Wan J. Microstructure and corrosion resistance of TiN/TiO<sub>2</sub> nano-composite film on AZ31 magnesium alloy. *Surf Coat Tech.* 2021;406:126681.
42. Luiz LA, Kurelo B, Souza GB, Andrade J, Marino CEB. Effect of nitrogen plasma immersion ion implantation on the corrosion protection mechanisms of different stainless steels. *Mater Today Commun.* 2021;28:102655.
43. Li Y, Bi Y, Zhang M, Zhang S, Gao X, Zhang Z, et al. Hollow cathodic plasma source nitriding of AISI 4140 steel. *Surf Eng.* 2021;37(3):351-9.
44. Cardoso W, Di Felice R, Baptista R, Machado TAP, Galdino AGS. Evaluation of the use of blast furnace slag as an additive in mortars. *REM Int Eng J.* 2022;75(3):215-24.

45. Mahadule D, Khatirkar RK, Gupta SK, Gupta A, Dandekar TR. Microstructure evolution and corrosion behaviour of a high Mo containing  $\alpha + \beta$  titanium alloy for biomedical applications. *J Alloys Compd.* 2022;912:165240.
46. Naeem M, Awan S, Shafiq M, Raza HA, Iqbal J, Díaz-Guillén JC, et al. Wear and corrosion studies of duplex surface-treated AISI-304 steel by a combination of cathodic cage plasma nitriding and PVD-TiN coating. *Ceram Int.* 2022;48(15):21473-82.
47. Taherkhani K, Soltanieh M. Investigation of nanomechanical and adhesion behavior for AlN coating and AlN/3N-Fe<sub>2</sub> composite coatings created by Active Screen Plasma Nitriding on Al 1050. *J Alloys Compd.* 2019;783:113-27.
48. Cardoso W, Di Felice R, Santos BN, Schitine AN, Machado TAP, Galdino AGS, et al. Modeling of artificial neural networks for silicon prediction in the cast iron production process. *IAES Int J Artif Intell.* 2022;11(2):530-8.
49. Nogueira JW Jr, Monção RM, Bandeira RM, et al. Growth of  $\alpha$ -Fe<sub>2</sub>O<sub>3</sub> thin films by plasma deposition: studies of structural, morphological, electrochemical, and thermal-optical properties. *Thin Solid Films.* 2021;736:138919.
50. Sousa RRM, Araújo FO, Costa JAP, Dumelow T, Oliveira RS, Alves C Jr. Nitriding in cathodic cage of stainless steel AISI 316: influence of sample position. *Vacuum.* 2009;83(11):1402-5.
51. Sriraman KR, Straus HW, Brahimi S, Chromik RR, Szpunar JA, Osborne JH, et al. Tribological behavior of electrodeposited Zn, Zn-Ni, Cd and Cd-Ti coatings on low carbon steel substrates. *Tribol Int.* 2012;56:107-20.
52. Cardoso W, Di Felice R, Baptista R. Artificial neural network-based committee machine for predicting the slag quality of a blast furnace fed with metallurgical coke. In: 7th Brazilian Technology Symposium, BTSym; 2021 Nov 8-10; Campinas, Brazil. Proceedings. Cham: Springer Nature; 2021. p. 66-73.
53. Morell-Pacheco A, Kim H, Wang T, Shiao CH, Balerio R, Gabriel A, et al. Ni coating on 316L stainless steel using cage plasma treatment: feasibility and swelling studies. *J Nucl Mater.* 2020;540:152385.
54. Piasecki A, Kulka M, Kotkowiak M. Wear resistance improvement of 100CrMnSi6-4 bearing steel by laser boriding using CaF<sub>2</sub> self-lubricating addition. *Tribol Int.* 2016;97:173-91.
55. Wang L, Li Y, Wu X. Plasma nitriding of low alloy steels at floating and cathodic potentials. *Appl Surf Sci.* 2008;254(20):6595-600.
56. Ostrovskaya O, Badini C, Deambrosio SM, Miorin E, Biamino S, Padovano E. Protection from oxidation of second and third generation TiAl intermetallic alloys by magnetron sputtering deposition of a TiAl/TiAlN coating. *Mater Des.* 2021;208:109905.
57. Pinedo CE, Larrotta SI, Nishikawa AS, Dong H, Li X-Y, Magnabosco R, et al. Low temperature active screen plasma nitriding of 17-4 PH stainless steel. *Surf Coat Tech.* 2016;308:189-94.
58. Cardoso W, Di Felice R. Forecast of carbon consumption of a blast furnace using extreme learning machine and probabilistic reasoning. *Chem Eng Trans.* 2022;96:493-8.
59. Saeed A, Khan AW, Jan F, Abrar M, Khalid M, Zakaullah M. Validity of "sputtering and re-condensation" model in active screen cage plasma nitriding process. *Appl Surf Sci.* 2013;273:173-8.
60. Sousa EM, Leitão ABV, Serra PLC, Borges JO, Vega ML, Moura JVB, et al. Surface modification of AISI 316 steel by  $\alpha$ -MoO<sub>3</sub> thin films grown using cathodic cage plasma deposition. *Physica B.* 2003;648:414410.
61. Li H, Sun P, Cheng D. Structure and properties of a-C:H:Si:O films deposited by cage-like hollow cathode discharge on AZ31 alloy. *Tribol Int.* 2022;175:107848.
62. Li Y, He Y, Wang W, Mao J, Zhang L, Zhu Y, et al. Plasma nitriding of AISI 304 Stainless steel in cathodic and floating electric potential: influence on morphology, chemical characteristics and tribological behavior. *J Mater Eng Perform.* 2018;27(3):948-60.
63. Libório MS, Praxedes GB, Lima LLF, Nascimento IG, Sousa RRM, Naeem M, et al. Surface modification of M2 steel by combination of cathodic cage plasma deposition and magnetron sputtered MoS<sub>2</sub>-TiN multilayer coatings. *Surf Coat Tech.* 2020;384:125327.
64. Liu HY, Che HL, Gao JY, Li GB, Lei MK. Low-pressure hollow cathode plasma source carburizing of AISI 304L austenitic stainless steel at low temperature. *Surf Coat Tech.* 2022;442:128548.
65. Naeem M, Iqbal J, Zakaullah M, Shafiq M, Mujahid ZI, Díaz-Guillén JC, et al. Enhanced wear and corrosion resistance of AISI-304 steel by duplex cathodic cage plasma treatment. *Surf Coat Tech.* 2019;375:34-45.
66. Naeem M, Khan KH, Shahid M, Iqbal J, Shafiq M, Zaka-ul-Islam M, et al. Non-intrusive measurement of electron, vibrational, rotational temperatures and active species concentration in N<sub>2</sub>-H<sub>2</sub> cathodic cage plasma. *Surf Coat Tech.* 2018;344:233-43.
67. Ribeiro KJB, Sousa RRM, Araújo FO, Brito RA, Barbosa JCP, Alves C Jr. Industrial application of AISI 4340 steels treated in cathodic cage plasma nitriding technique. *Mater Sci Eng A.* 2008;479(2):142-7.
68. Rocha RC, Galdino AGS, Silva SN, Machado MLP. Surface, microstructural, and adhesion strength investigations of a bioactive hydroxyapatite-titanium oxide ceramic coating applied to Ti-6Al-4V alloys by plasma thermal spraying. *Mater Res.* 2018;21(4):e20171144.
69. Russo F, Fontanari V, Rossi S. Abrasion behavior and functional properties of composite vitreous enamel coatings fabricated with the addition of 316L stainless steel flakes. *Ceram Int.* 2022;48(16):23666-77.
70. Sousa FA, Costa JAP, Sousa RRM, Barbosa JCP, Araújo FO. Internal coating of pipes using the cathodic cage plasma nitriding technique. *Surf Interfaces.* 2020;21:100691.
71. Sousa FA, Costa JAP, Sousa RRM, Barbosa JCP, Araújo FO. Internal coating of pipes using the cathodic cage plasma nitriding technique. *Surf Interfaces.* 2020;21:100691.
72. Cardoso W, Di Felice R, Baptista R. Mathematical modelling to predict fuel consumption in a blast furnace using artificial neural networks. In: International Conference on Intelligent Emerging Methods of Artificial Intelligence & Cloud Computing. IEMAICLOUD 2021. Smart Innovation, Systems and Technologies; 2022; London, UK. Proceedings. Cham: Springer Nature; 2022.
73. Cardoso W, Di Felice R. Prediction of silicon content in the hot metal using Bayesian networks and probabilistic reasoning. *Int J Adv Intell Inf.* 2021;7(3):268-81.